ELSEVIER

Journal of Nuclear Materials 278 (2000) 149–163

journal of nuclear materials

www.elsevier.nl/locate/jnucmat

Variability of radiation-induced segregation in iron–chromium–nickel alloys

T.R. Allen [a,*], E.A. Kenik [b], G.S. Was [c]

[a] *Argonne National Laboratory – West, P.O. Box 2528, Idaho Falls, ID 83403-2528, USA*

[b] *Metals and Ceramics Division, Oak Ridge National Laboratory, Oak Ridge, TN 37831, USA*

[c] *Department of Nuclear Engineering and Radiological Sciences, University of Michigan, Ann Arbor, MI 48109, USA*

Received 4 June 1999; accepted 20 October 1999

Abstract

This work examines the variability in grain boundary segregation measurements in proton irradiated iron–chromium–nickel alloys made using Auger electron spectroscopy (AES) and scanning transmission electron microscopy with energy dispersive X-ray spectroscopy (STEM-EDS). Variability occurs in segregation measurements made on different boundaries in the same sample and made on different samples irradiated under the same conditions. Variability occurs in each measurement technique, but is greater for AES. A portion of the greater variability in the AES measurements occurs because only the concentrations calculated from AES measurements are sensitive to changes in the shape of the energy intensity peak. A statistical analysis technique for testing the consistency of experimental conditions demonstrated that the variability is not attributable to uncertainty in irradiation temperature, dose, or material condition. Finally, the analysis of grain boundary composition distributions in Fe–20Cr–9Ni indicates that attempts to minimize environmental cracking by controlling grain boundary composition need to focus on both the average grain boundary compositions and the shape of the concentration distributions.

1. Introduction

Radiation-induced segregation (RIS) at grain boundaries in iron–chromium–nickel alloys is important because of its implications to irradiation-assisted stress corrosion cracking in water reactors [1–9]. To better understand the segregation process, a broad study of RIS in proton irradiated austenitic iron–chromium–nickel alloys was performed [10]. In the study, grain boundary composition was measured using both Auger electron spectroscopy (AES) and scanning transmission electron microscopy with energy dispersive X-ray spectroscopy (STEM-EDS). Grain boundary composition measurements were found to vary between boundaries in the same sample and between samples with the same processing and radiation history. Since cracking susceptibility may be related to grain boundary composition, an understanding of this variability is important.

Scatter in measurement of grain boundary segregation can be caused by three factors: extrinsic sample history effects such as differences in preparation or irradiation dose or temperature; intrinsic material effects such as alloy composition, grain boundary orientation, and elemental diffusivity; and measurement uncertainties such as spectral interpretation, analysis beam quality, or sample contamination. Extrinsic sample history effects can contribute to differences in the measured segregation. If samples are unintentionally irradiated at different temperatures, to different doses, or do not have the same starting condition due to differences in processing, the measured segregation is expected to be different. To ensure that experimental conditions are consistent between samples, the temperature and dose are measured during irradiation. Additionally,

* Corresponding author. Tel.: +1-208 533 7760; fax: +1-208 533 7863.

E-mail address: todd.allen@anlw.anl.gov (T.R. Allen).

0022-3115/00/$ - see front matter
PII: S0022-3115(99)00263-9

post-irradiation statistical analysis of β^-decay can be performed to confirm that differences in experimental condition did not lead to differences in segregation.

Intrinsic material effects can alter the segregation process, creating scatter in measured grain boundary segregation. Briant [11] previously described the variability in grain boundary segregation in non-irradiated materials. Using grain boundary compositions measured with AES, he noted that scatter on a single boundary is much smaller than scatter between boundaries in the same sample. Boundary-to-boundary comparisons revealed that the majority of the segregation lies within ±30% of the average value. Briant analyzed five different sources of variation: angular variations among different grain boundary facets with respect to the cylindrical mirror analyzer, variations produced by the fracture process, variations which result from compositional inhomogeneity within the matrix, variations caused by not allowing segregation to reach equilibrium, and variations caused by differences in grain boundary structure. He showed that angular variations with respect to the analyzer did not contribute significantly to compositional variation and that while fracture does introduce a small amount of scatter in the measurements, it is not sufficient to account for all of the compositional variation. Briant postulated that compositional inhomogeneity, non-equilibrium segregation, and differences in grain boundary structure could all contribute significantly to compositional variation. Similar mechanisms could also affect segregation in irradiated alloys. Compositional inhomogeneity and variable grain boundary structure can occur in any alloy. Since RIS is a non-equilibrium process, an equilibrium state is never reached, rather a steady-state condition is eventually achieved. Variation in grain boundary composition can be caused by differences in the rate of approach to steady state.

Carter et al. [12] examined the difference between AES and STEM-EDS by analyzing ultra-high purity stainless steel irradiated with protons. They outlined the limitations of each method that can produce variability.

In STEM, errors in measurement can arise due to electron beam broadening in the foil, inaccurate measurement of foil thickness, insufficient counting time (poor statistics), sample drift during spectrum collection, contamination by surface films, improper accounting for spurious radiation, and the lack of a sufficient number of spectra to average boundary-to-boundary variations in composition. Errors in AES measurements occur due to the overlap of peaks from different elements, insufficient counting time (poor statistics), improper alignment of the grain facet relative to the cylindrical mirror analyzer, improper identification of intergranular (IG) facets, fracture near but not in the grain boundary plane, precipitation of grain boundary phases, unequal distribution of impurities between the two fracture surfaces, sample drift during analysis, the lack of a sufficient number of spectra to average boundary-to-boundary variations in composition, and contribution from several atom layers due to the finite Auger electron escape depth.

Carter et al. showed that AES consistently measures 1–3 at.% more chromium depletion than STEM-EDS and that this difference was expected from the difference in the resolution of the techniques. Although Carter provided a detailed analysis of differences in average segregation measured using each technique, a detailed analysis of the scatter using each technique was not performed.

In this work, an additional explanation, based on peak shape effects, is provided for the greater scatter in AES measurements as compared to STEM-EDS measurements. Additionally, a statistical analysis technique is presented to examine the effect of radiation history on variability in grain boundary composition. This analysis will show that variability in measured segregation between proton irradiated samples is not caused by systematic differences in irradiation conditions. Finally, a statistical analysis is used to examine how variability in segregation in an Fe–20Cr–9Ni alloy can affect material properties such as environmental cracking and swelling.

2. Experiment

In previous related studies, grain boundary compositions were measured using AES on four alloys: Ni–18Cr, Ni–18Cr–9Fe, Ni–18Cr–0.08P, and Fe–20Cr–9Ni at temperatures between 200°C and 500°C and doses between 0.1 and 1.0 dpa [10]. For Ni–18Cr and Ni–18Cr–9Fe, grain boundary compositions were also measured using STEM-EDS for samples irradiated at 400°C to doses from 0.1 to 1.0 dpa. AES and STEM-EDS measurements were also taken on unirradiated grain boundaries for the respective alloys. In all, over 800 grain boundary composition measurements have been made. The details of the irradiation and analysis procedure are described in detail in Refs. [8,13].

This paper will examine how measurement technique and material condition (caused by experimental temperature and dose) affect segregation variability and examine the effect of this segregation variability on material properties such as irradiation assisted stress corrosion cracking (IASCC) and void swelling. A brief description of composition determination using AES and STEM-EDS is provided below. Three different statistical measures will be used to examine variability in grain boundary composition measurements. A description of each statistical technique follows.

2.1. AES measurements

AES samples were analyzed in a Phi 660 scanning Auger microprobe (SAM) located at Ford Research and Development Center, Dearborn, MI. The grain boundaries chosen to be analyzed were located away from the surface to minimize the effect of surface segregation and oxidation during irradiation. The grain facets analyzed were at least 5 μm in diameter to allow for some sample drift while maintaining the microprobe on the grain facet. The electron beam was rastered over an area typically one half the area of the grain boundary facet and spectra collected from the entire area of beam raster. All energy intensity spectra (frequency of Auger electrons detected in each energy band) were collected using an electron beam energy of 10 keV. Samples were analyzed in the multiplex mode of the SAM, scanning for Fe, Cr, Ni, P, C, and O as appropriate for the sample being analyzed. C and O were analyzed to monitor the status of contamination to the exposed grain boundary facets. Because of overlap between the 529 eV Cr peak and the 513 eV O peak, data collection for each sample was terminated if the calculated O concentrations approached 15–20 at.%, limiting data collection to between 8 and 20 grain boundaries per sample for an analysis period of about 2 h. Damcott et al. [8] showed that the measured oxygen concentration can reach levels of around 20 at.% without causing a measurable change in measured chromium concentration.

In AES, the grain boundary concentration is calculated from the measured energy intensities using the following relationship [14]:

$$C_i = \frac{I_i/\lambda_i}{\sum(I/\lambda)}, \tag{1}$$

where I is the intensity of the signal for element i (as determined by the peak-to-peak height of the differentiated AES spectra) and λ is the relative sensitivity factor. In AES, intensity profiles were not used to directly calculate concentrations. Because of the large background signal of backscattered and secondary electrons present at the detector in a scanning Auger microprobe, the intensity peaks of the Auger electrons can be difficult to discern. Therefore, the intensity profile is differentiated with respect to energy to highlight the Auger peaks, and the peak-to-peak height of the differentiated spectrum is used as a measure of the intensity of each peak. The peak-to-peak height of the differentiated spectrum is assumed to be proportional to the area under the intensity profile (this relationship is exact if the intensity profile is Gaussian in shape). If the AES intensity peaks change shape from boundary-to-boundary, use of the differentiated peak-to-peak height may generate greater uncertainty when calculating concentrations.

2.2. STEM-EDS measurements

STEM-EDS was performed at Oak Ridge National Laboratory using a Phillips EM400T/FEG equipped with an EDAX 9100/70 EDS system. An accelerating voltage of 100 kV was used. STEM-EDS measurements were performed at the grain boundary and at increments of 2.5 nm away from the boundary to yield composition profiles. The incident probe thickness was 2 nm (full width, tenth maximum). The sample is tilted toward the X-ray detector and each grain boundary analyzed is aligned such that the boundary is 'edge-on' (parallel to the electron beam). This placement ensures that the measured X-ray intensity has equal contributions from both sides of the boundary. The grain boundary is located by placing the electron probe in a position that generates equal portions of the diffraction patterns from each side of the boundary. Data acquisition lasted for 100 s of detector live time with X-ray counting rates of 1000–2000 counts per second.

The concentration is calculated from the relative intensities for each element. For the alloys in this study, X-ray intensities were collected for the K_α peaks of Fe (7.114 keV), Cr (5.989 keV), and Ni (8.333 keV). The ratio of the concentration of two atoms is proportional to the ratio of the measured intensities, with the proportionality constant known as the k-factor

$$\frac{C_A}{C_B} = k_{AB}\frac{I_A}{I_B} \quad \text{and} \quad \frac{C_B}{C_C} = k_{BC}\frac{I_B}{I_C}. \tag{2}$$

Assuming that

$$C_A + C_B + C_C = 1, \tag{3}$$

(no other elements exist), the concentrations are calculated by simultaneously solving Eqs. (2) and (3). To calculate the k-factors, concentrations in the bulk of the material, away from the grain boundary, are measured. The k-factor is chosen such that this bulk concentration measurement corresponds to the bulk concentration as measured by electron microprobe:

$$k_{AB} = \frac{C_A^{\text{microprobe}}}{C_B^{\text{microprobe}}}\frac{I_B^{\text{STEM-EDS}}}{I_A^{\text{STEM-EDS}}}. \tag{4}$$

A separate k-factor is calculated for each irradiated TEM disk.

2.3. Statistical analysis techniques

Differences in sample-to-sample averages will be examined using t-tests and differences in sample-to-sample variance will be examined using F-tests. Both t- and F-tests are used to examine the statistical significance of differences in measured segregation. Statistically significant differences in measured segregation are a motive for further examination of the measurements and

experiment. Shapes of distributions will be examined using kurtosis and CDFs as the analysis tools. RIS has been implicated as a contributor to stress corrosion cracking and void swelling susceptibility. In determining the effect of RIS, both the average segregation and the distribution about the average are important. The use of kurtosis as a measure of spread from the mean and the relationship to stress corrosion cracking and void swelling will be examined in a later section. Each of these tests are described below.

2.3.1. Comparison of means

The differences in average grain boundary concentration between samples can be examined statistically. Specifically, the sample averages can be tested to determine if sufficient evidence exists to indicate that they are not from the same sample population (same alloy, temperature, and dose). For data sets where each sample average is drawn from a small number (typically less than 30 of grain boundary measurements, the Student's t-distribution is appropriate [15]. The Student's t-distribution is given in Fig. 1(a) which plots the t-distribution along with the more familiar normal distribution (the normal distribution would be appropriate for large sample sizes).

The difference between two sample means are compared as follows. The null hypothesis H_0 is defined as the two sample means being equal

$$H_0 : \mu_1 = \mu_2, \tag{5}$$

where μ is the sample mean. To test the null hypothesis, a test statistic β is calculated and compared to the t-distribution. The test statistic β is a measure of the difference between averages relative to the spread of the measurements. The test statistic β is defined as

$$\beta = \frac{\overline{y_1} - \overline{y_2}}{s\sqrt{\frac{1}{n_1} + \frac{1}{n_2}}}, \tag{6}$$

where y is the sample average, s the pooled estimator of the standard deviation (pooled indicating that both samples are used to determine the standard deviation), and n is the number of measurements contributing to each sample average. The test statistic β is large if the difference between sample averages is large compared to the spread in the measurements. When calculating s, each set of measurements is assumed to have the same standard deviation and the best estimate of the population standard deviation is the pooled estimate from both sample sets. This estimator is based on the sum of squares errors and is defined as

$$s^2 = \frac{\sum_{i=1}^{n_1} (y_i - \overline{y_1})^2 + \sum_{i=1}^{n_2} (y_i - \overline{y_2})^2}{n_1 + n_2 - 2}. \tag{7}$$

If the difference between the sample means $(\overline{y_1} - \overline{y_2})$ is large compared to the standard deviation (s), then statistically, the sample averages are not equal.

For each comparison of sample means, the test statistic β is calculated and compared to a t-distribution. From the t-distribution, a confidence interval is defined (for instance a 95% confidence interval) and the values $\pm t_\alpha$ (where $\alpha = 5\%$) which define the boundaries of the confidence interval are calculated (see Fig. 1(b)). If the test statistic β falls outside the region of confidence ($\beta < -t_{\alpha/2}$ or $\beta > t_{\alpha/2}$), then we reject the hypothesis that the sample averages are equal. For this work, a 95% confidence interval is used for all calculations.

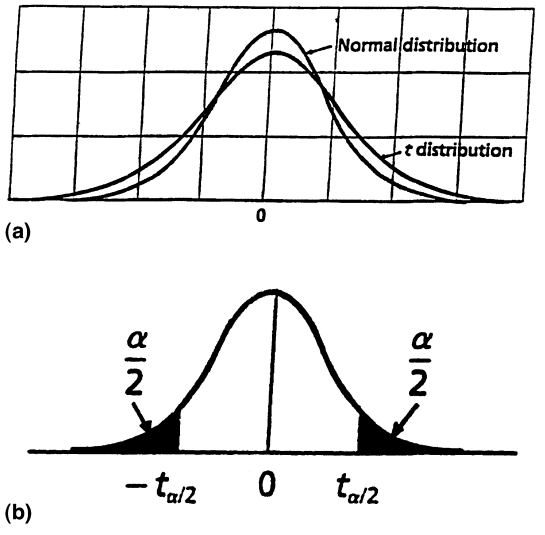

Fig. 1. (a) The Student's t-distribution. (b) The Student's t-distribution showing the rejection region (shaded areas).

2.3.2. Comparison of variance

In samples of the same material, with the same processing and radiation history, the spread of measurements about the average should be similar. Differences in the variance indicate dissimilar histories. Sample-to-sample differences can be statistically examined by comparing the variance of each sample. The standard test for comparing the variance of two different samples is the F-test [15]. An example of the F-distribution is given in Fig. 2. Similar to the t-distribution tests, we test the null hypothesis that the variances of two samples are equal

$$H_0 : \sigma_1^2 = \sigma_2^2, \tag{8}$$

where σ is the population standard deviation. The F-test compares the ratio of the sample variance (the variance is the square of the standard deviation). The test statistic Φ is defined as the ratio

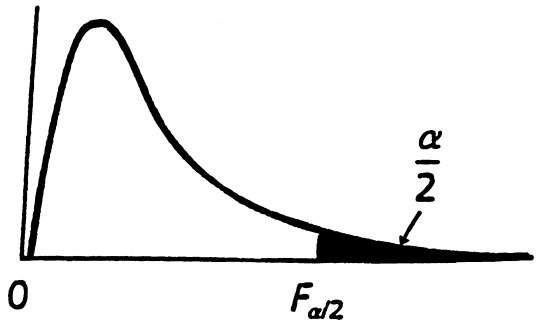

Fig. 2. The F-distribution showing the rejection region (shaded area).

$$\Phi = \frac{s_1^2}{s_2^2}, \tag{9}$$

where s is the standard deviation for a single sample. If s_1 is much larger than s_2, the test statistic Φ will be large. A confidence interval in the F-distribution is defined (a 95% confidence interval is used). If the test statistic Φ falls outside the limits defined by the confidence interval ($\pm F_{\alpha/2}$) (where $\alpha = 5\%$), the null hypothesis that the sample variances are equal is rejected.

2.3.3. Kurtosis and the cumulative distribution function

Information about the effects of segregation can be gained by looking at the distribution of concentration measurements. The concentration measurements can be plotted on a histogram, showing the relative frequency at which certain concentration measurements occur. Fig. 3(a) shows three different distributions (probability density functions), a normal distribution, a flat (or uniform) distribution, and a distribution more sharply peaked than the normal distribution. The degree of peakedness of a distribution is known as the kurtosis (or moment of kurtosis, α_4). The kurtosis is defined mathematically as

$$\alpha_4 = \frac{\sum_{j=1}^{N} \left(X_j - \bar{X}\right)^4}{N\sigma^4}, \tag{10}$$

where N is the number of measurements, X_j the individual measurements, $\bar{X}$ the mean concentration, and σ is the standard deviation. *The larger the kurtosis, the more sharply peaked is the distribution.* For two distributions with the same variance, a more positive kurtosis indicates that more cases cluster about a central point with more observations straggling into the extreme tails of the distribution. In many cases, the kurtosis is reported relative to a normal distribution, which has a moment of kurtosis equal to 3.

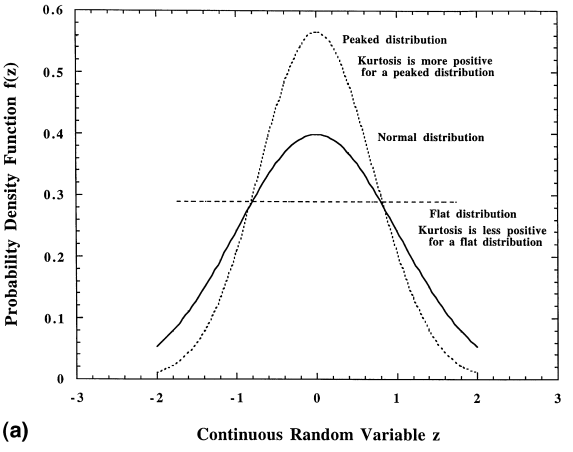

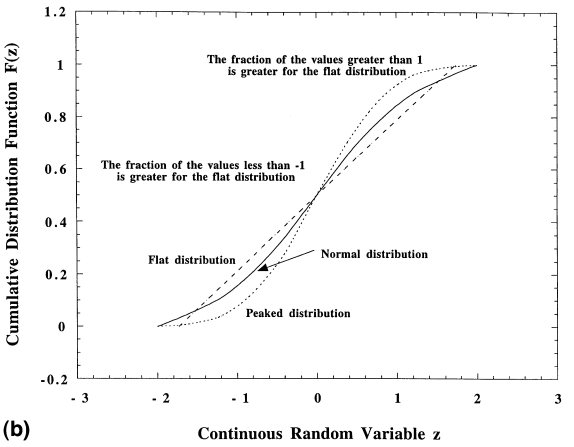

Fig. 3. (a) Probability density functions for a flat, normal, and peaked distribution. (b) Cumulative distribution functions for the PDFs in Fig. 1(b).

The kurtosis is important in that it is related to the probability that a measured concentration is less than or greater than a critical value (e.g., a minimum grain boundary chromium concentration below which cracking will occur). This can be seen by plotting the cumulative distribution function (CDF), which is the integral of the probability density function. The CDF provides the probability that a measurement is less than a certain value. The CDFs for the distributions in Fig. 3(a) are plotted in Fig. 3(b). For distributions flatter than a normal distribution (the 'flat distribution' in Fig. 3(a)), a greater number of measurements are located far from the mean. For a negative value of the random variable z, a larger fraction of measurements are less than z in the flat distribution. For a positive value of the random variable z, a larger fraction of measurements are greater than z in the flat distribution. For the distribution that is more peaked than the normal distribution, fewer measurements are found far from the mean.

3. Variability in measured grain boundary concentration

Fig. 4 shows the measured (using AES) grain boundary chromium composition for the Ni–18Cr alloy irradiated at 400°C as a function of dose. The individual measurements, along with the sample averages are shown. The data from different samples at each dose are separated for clarity. Data points along a vertical line are all measurements from the same sample and represent the boundary-to-boundary scatter within a single sample. The uncertainty bars indicate the standard deviation for the sample. For each dose, composition measurements are provided from at least two separate samples. Considerable scatter exists in average grain boundary composition for samples irradiated at the same dose. This scatter is typical for all of the alloys examined. Fig. 5 shows the grain boundary chromium composition, as measured using AES and STEM-EDS, for the Ni–18Cr alloy irradiated at 400°C as a function of dose. The AES measurements are the same as plotted in Fig. 4. The scatter is generally larger in the AES measurements. Larger scatter in the AES measurements is typical for all the alloys examined. The *F*-test can be used to statistically substantiate the larger scatter in AES measurements. Table 1 compares the variance between AES and STEM-EDS measurements for the Ni–18Cr and Ni–18Cr–9Fe alloys. The variance calculated from AES measurements is always greater than or equal to that of the STEM-EDS measurements.

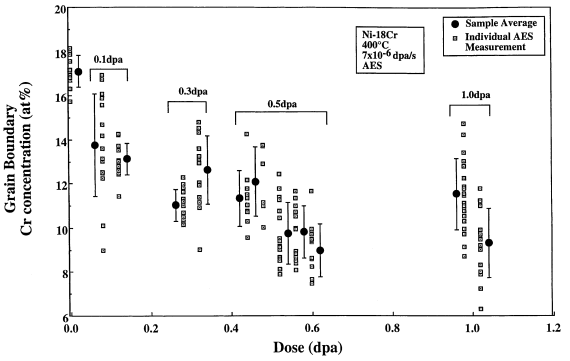

Fig. 4. Grain boundary chromium composition, as measured using AES, for the Ni–18Cr alloy irradiated at 400°C as a function of dose. The data from different samples at each dose are separated for clarity.

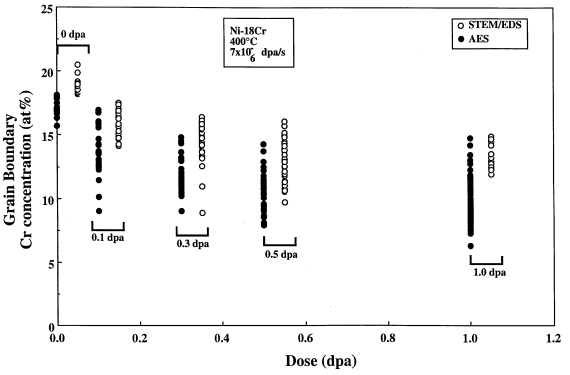

Fig. 5. Grain boundary chromium composition, as measured using AES and STEM-EDS, for the Ni–18Cr alloy irradiated at 400°C as a function of dose.

4. Variability due to analysis instrument (measurement uncertainties)

The data scatter in AES measurements is typically larger than the scatter in STEM-EDS measurements. The difference in variability between AES and STEM–EDS measurements can be understood in the context of how compositions are computed in each technique. Of the two techniques, the AES concentration calculation,

Table 1
Statistical analysis of sample variance between AES and STEM-EDS measurements in the Ni–18Cr and Ni–18Cr–9Fe alloys

Irradiation condition	STEM-EDS variance	AES variance	Test statistic Φ	Confidence interval F_α (95%)	Is the AES variance statistically different than the STEM-EDS ($\Phi > F_\alpha$)
Ni–18Cr (*temp.*, *dpa*)					
0	0.38	0.50	1.32	2.51	Statistically equal
400°C, 0.1	0.97	2.75	2.83	1.95	AES variance greater
400°C, 0.3	2.15	2.06	1.05	1.79	Statistically equal
400°C, 0.5	2.67	2.62	1.02	1.63	Statistically equal
400°C, 1.0	1.02	3.66	3.61	2.29	AES variance greater
Ni–18Cr–9Fe					
0	0.56	0.73	1.30	2.37	Statistically equal
400°C, 0.1	0.78	1.38	1.76	1.98	Statistically equal
400°C, 0.3	0.67	3.22	4.81	2.10	AES variance greater
400°C, 0.5	1.96	1.46	1.34	1.87	Statistically equal
400°C, 1.0	0.59	2.48	4.17	1.98	AES variance greater

which uses the derivative of the intensity spectra to calculate concentrations, is far more sensitive to intensity peak shape. Small changes in the peak shape (possibly due to differences in sample-detector geometry, chemical effects, or inadequate counting statistics) can have a significant effect on the calculated concentration. In contrast, only the area under the intensity curve is used to calculate the concentration from the X-ray intensity using STEM-EDS, making the calculation less sensitive to peak shape.

To illustrate the effect, Fig. 6(a) shows two Gaussian profiles and Fig. 6(b) shows the differentiated spectra of the Gaussians in Fig. 6(a). The height and width of the two Gaussian profiles are different, but the areas under each of the Gaussian curves are equal. For a 0.1 eV (3%) difference in width, the height of the narrower profile is approximately 3% larger. As the differentiated profiles show, the wider the intensity profile, the smaller the peak-to-peak height in the differential spectra. The 0.1 eV difference in width of the Gaussian profiles leads to a 5% difference in peak-to-peak height of the differentiated profiles. Thus, if peak-to-peak heights of the differentiated curves are used to determine the intensity, as in AES measurements, then the narrower Gaussian gives a larger intensity. However, if areas under the intensity curve are used to calculate X-ray intensity, as in STEM-EDS calculations, then both curves in Fig. 6(a) would give the same intensity.

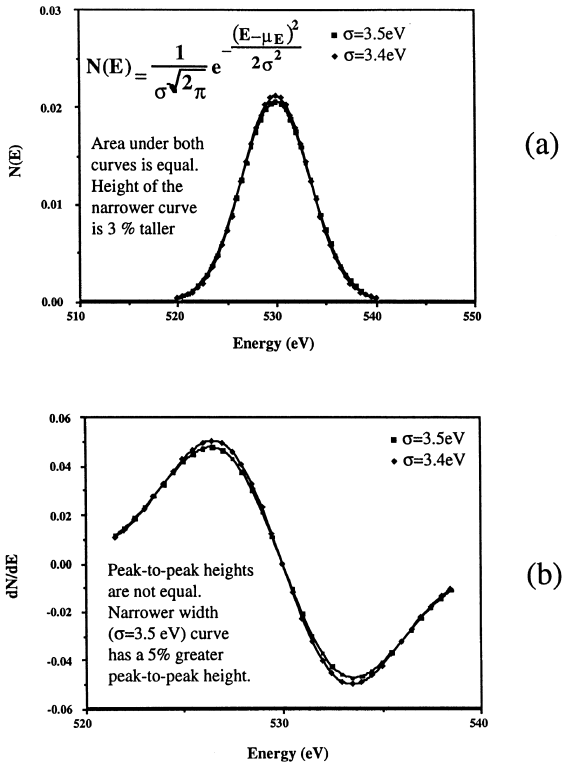

Fig. 6. (a) Two Gaussian profiles centered on 530 eV. The width of the two profiles (expressed as the standard deviation σ) are different, but the area under the curves are equal. The average energy (μ_E) for both curves is 530 eV. (b) The curves from Fig. 4(a), differentiated with respect to energy. The peak-to-peak heights are not equal.

Chemical effects, differences in sample-detector geometry, or inadequate counting statistics may cause small changes in peak shape. For example, the proportionality between the peak-to-peak height and the area under the intensity profiles is not exact if the peak shape differs from the standard peak used to calculate the sensitivity factors. This difference can occur if the shape of the intensity profile is affected by chemical interactions between atoms in the lattice. Such problems have been observed when measuring an element present in a thin film [16]. In addition, since the energy loss through the lattice varies with the energy of the particular Auger electron, the structure of the grain boundary and the shape of the grain boundary facet can alter the shape of the intensity profile for the emitted electrons. These surface roughness effects can change the measured intensity in two ways [17]. As the angle between the incident electron beam becomes more grazing, the number of emitted Auger electrons increases, because more

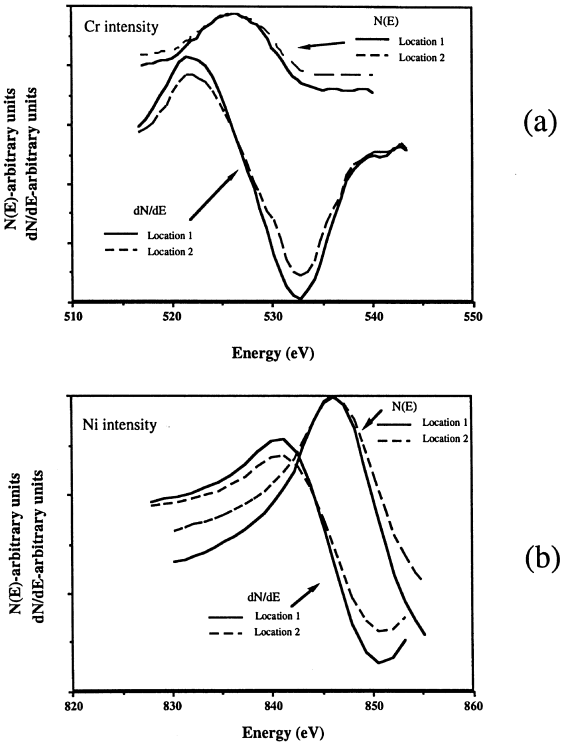

Fig. 7. (a) The intensity profiles and differentiated intensity profiles for Cr from two areas on the same grain boundary. (b) The intensity profiles and differentiated intensity profiles for Ni from two areas on the same grain boundary.

ionization occurs within the escape depth of the Auger electrons. This effect depends on the elements in the alloy because the Auger electron energy is element dependent. Also, as the angle between the surface normal and the detector increases, fewer electrons are collected at the detector. Finally, insufficient counting times, which give incomplete statistics, can alter the shape of the intensity profile.

As an example of peak shape effects in actual measurements, two measurements were taken jointly on different locations of the same boundary in a sample of the Ni–18Cr alloy. The intensity profiles and the differential profiles are given in Fig. 7(a) for Cr and 7(b) for Ni. As the figures show, Location 2 has broader peaks than Location 1. This difference shows up as smaller peak-to-peak height differences in the differential spectra. The difference in peak shape is not the same for the Cr and the Ni peaks. While the difference in Cr peak shape between the two areas is small, the Ni peak for Location 2 is significantly broader than the Ni intensity profile for Location 1. As a result, the calculated Cr concentration for Location 2 is about 0.4 at.% higher

Table 2
Statistical analysis of sample averages in the Ni–18Cr, Ni–18Cr–9Fe, Ni–18Cr–0.08P and Fe–20Cr–9Ni

Condition	Sample average		Test statistic β	Confidence region t_α (95%)	Are sample averages statistically equal ($\beta < t_\alpha$)
Ni-18Cr (*temp.*, *dpa*)					
200°C, 0.5	15.15	14.12	2.28	2.056	No
300°C, 0.5	12.24	10.59	4.19	1.96	No
500°C, 0.5	13.76	11.81	2.14	2.08	No
400°C, 0.1	13.14	13.75	1.06	1.960	Yes
400°C, 0.3	12.63	11.03	3.83	1.960	No
400°C, 0.5	12.09	11.35	1.04	2.145	Yes
400°C, 0.5	12.09	9.76	3.37	2.086	No
400°C, 0.5	12.09	9.82	3.65	2.093	No
400°C, 0.5	12.09	8.98	5.01	2.093	No
400°C, 0.5	11.35	9.76	2.91	2.064	No
400°C, 0.5	11.35	9.82	3.10	2.069	No
400°C, 0.5	11.35	8.98	4.82	2.069	No
400°C, 0.5	9.76	9.82	0.13	2.045	Yes
400°C, 0.5	9.76	8.98	1.69	2.045	Yes
400°C, 0.5	9.82	8.98	1.99	2.048	Yes[a]
400°C, 1.0	11.53	9.32	4.14	1.960	No
Ni–18Cr–9Fe					
0	18.1	17.8	0.57	2.228	Yes
400°C, 0.1	13.6	14.4	1.56	2.080	Yes
400°C, 0.3	13.7	14.5	1.14	2.080	Yes
400°C, 0.5	13.2	13.8	1.25	2.060	Yes
400°C, 1.0	13.3	14.3	1.89	2.052	Yes
500°C, 0.5	15.7	15.5	0.44	2.056	Yes
Ni–18Cr–0.08P					
400°C, 0.5	8.65	8.65	0.005	2.074	Yes
Fe–20Cr–9Ni					
400°C, 0.1	21.7	20.8	1.61	2.069	Yes
400°C, 1.0	15.8	17.7	4.05	2.060	No
400°C, 1.0	15.8	18.1	4.23	2.052	No
400°C, 1.0	15.8	16.5	1.57	2.060	Yes
400°C, 1.0	15.8	16.7	1.25	2.060	Yes
400°C, 1.0	17.7	18.1	0.60	2.064	Yes
400°C, 1.0	17.7	16.5	2.19	2.074	No
400°C, 1.0	17.7	16.7	1.39	2.074	Yes
400°C, 1.0	18.1	16.5	2.82	2.064	No
400°C, 1.0	18.1	16.7	1.94	2.064	Yes
400°C, 1.0	16.5	16.7	0.15	2.074	Yes
400°C, 3.0	8.72	9.42	0.99	2.069	Yes

[a] The samples with average Cr concentration of 9.82 and 8.98 at.% were originally a 4 mm TEM bar that was sectioned in half to make two 2 mm AES sample bars.

than that calculated for Location 1 (for a chromium concentration of 10 at.%).

5. Variability due to material history (extrinsic effects)

Samples with the same nominal irradiation history (irradiation dose, temperature, and sample preparation) should yield a similar material condition and have similar grain boundary concentrations. *t*-Tests can be used to compare average concentrations measured in samples with the same irradiation history. The results of *t*-tests comparing average Cr concentration in Ni–18Cr, Ni–18Cr–9Fe, Ni–18Cr–0.08P, and Fe–20Cr–9Ni samples are listed in Table 2. For each irradiation condition, samples that were irradiated to the same temperature and dose are paired to perform the *t*-test (samples may or may not have been irradiated on the same sample stage). For instance, the first line of Table 2 compares the sample averages from two Ni–18Cr samples that were irradiated at 200°C to 0.5 dpa. For Ni–18Cr irradiated at 400°C to 0.5 dpa, five samples were irradiated. Therefore, 10 combinations of sample pairs are analyzed. For each sample pair in Table 2, the sample averages, the test statistic β, and the confidence interval are listed. If the test statistic β falls within the confidence interval t_α, then the sample averages are statistically equal.

For Ni–18Cr–9Fe and Ni–18Cr–0.08P, all the sample pairs are statistically equal. For Fe–20Cr–9Ni, the majority of sample pairs have statistically equal averages. However, four of ten sample pairs irradiated to 1.0 dpa show statistically different averages. For Ni–18Cr, only the 400°C, 0.1 dpa samples and four of ten pairs of the 400°C, 0.5 dpa samples have the same average grain boundary concentration (the 400°C, 0.5 dpa samples with average Cr concentrations of 9.82 and 8.98 at.% were irradiated as a single sample which was subsequently cut in half to make two AES samples). Because of the statistically significant differences in sample average Cr concentration for Ni–18Cr, the sample temperature and dose histories must be examined more closely to determine if they can be the cause of the variability.

A systematic difference in temperature or dose caused by poor experimental control could lead to variability between samples expected to have the same radiation history. Because multiple samples are irradiated simultaneously, a systematic error would correspond with position on the irradiation stage. Up to eight samples are irradiated simultaneously on the irradiation stage (see Fig. 8). Stage position is identified by a number 1 through 8, with each stage position corresponding to a 2 mm wide position on the stage. Stage positions 1 and 8 are the left and right end positions, respectively, on the stage.

Examination of the sample position on the irradiation stage for each of the Ni–18Cr AES sample bars reveals an apparent systematic difference in segregation behavior. Table 3 lists the sample average Cr concentrations and stage positions for all the sample pairs irradiated on the same sample stage. For cases where the sample averages are not statistically equal (200°C, 0.5 dpa; 300°C, 0.5 dpa; 500°C, 0.5 dpa and 400°C, 0.3 dpa), stage position 1 shows less depletion (larger grain boundary Cr concentration) than position 5. The smaller depletion at position 1 could be due to a systematic difference in dose or temperature across the irradiation stage. The possibility of a systematic difference in temperature or dose suggested by the statistical analysis must be further investigated.

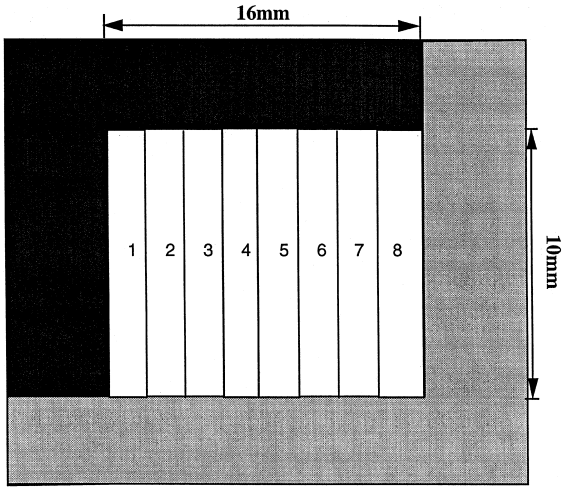

Fig. 8. Typical sample configuration on the irradiation stage.

5.1. Dose effects

Differences in dose from sample-to-sample in the same irradiation can be determined by counting the post-irradiation β^- activity. Table 3 shows the post-irradiation β^- counting for samples irradiated on the same irradiation stage. If the lesser segregation at stage position 1 was caused by a systematically lower dose (possibly due to the beam being blocked by the aperture or due to insufficient beam overscan), then the post-irradiation β^- counting rate should always be smaller for stage position 1. The counting data from Table 3 shows that the total dose is not systematically lower for sample position 1 compared to position 5.

Two more pieces of evidence indicate that differences in segregation are not due to differences in dose. The 400°C, 0.5 dpa samples with average concentrations of 8.98 and 9.82 at.% are AES samples that were sectioned from a single bar (and therefore had equal temperature and dose histories). These samples have differences in average grain boundary Cr concentration comparable to samples irradiated in different portions of the stage.

Table 3
Irradiation conditions for the Ni–18Cr samples irradiated on the same sample stage

Irradiation condition (temp., dpa)	Average Cr conc. for sample 1	Average Cr conc. for sample 2	Sample 1 stage position	Sample 2 stage position	Sample 1 β^- count rate (cpm)[a]		Sample 2 β^- count rate (cpm)[a]
200°C, 0.5	15.15	14.12	1	5	822.4 ± 9.1	<	1189.8 ± 10.9
300°C, 0.5	12.24	10.59	1	5	730.8 ± 8.5	>	701 ± 8.4
500°C, 0.5	13.76	11.81	1	5	534.5 ± 7.3		not counted
400°C, 0.1	13.14	13.75	1	5	194.6 ± 4.4	<	207.2 ± 4.6
400°C, 0.3	12.63	11.03	1	5	618.4 ± 7.9	<	629 ± 7.9
400°C, 0.5	12.09	11.35	5	8	665.8 ± 8.2	>	335.2 ± 5.8
400°C, 0.5	9.82	8.98	7,8[b]	7,8[b]	1345.4 ± 11.6		1345.4 ± 11.6

[a] Uncertainty in the counting rate calculated using $\sigma_r = \sqrt{\text{counting rate}/\text{counting time}}$ for a 10 min count.
[b] The samples with average Cr concentration of 9.82 and 8.98 at.% were originally a 4 mm TEM bar that was sectioned in half to make two 2 mm AES sample bars.

Additionally, the 400°C, 0.5 dpa samples with average grain boundary Cr concentration of 12.09 and 11.34 at.% indicate less segregation for the sample with larger dose (higher post-irradiation β^- count rate). Therefore, a significant difference in dose is not likely to be responsible for the sample-to-sample differences in average grain boundary Cr concentration.

5.2. Temperature effects

The variability in segregation measurements between stage positions 1 and 5 could be caused by a consistently under- or over-heated location on the irradiation stage. The effect of a systematic variation in temperature on Cr depletion can be examined using Fig. 9, which plots model calculations for the expected grain boundary Cr concentration in Ni–18Cr as a function of temperature. If the temperature of a sample in the 200°C irradiation was actually lower than 200°C, the expected grain boundary Cr concentration would be greater. Table 4 shows the effect of stage position 1 having a lower temperature than stage position 5 for the 200°C, 0.5 dpa; 300°C, 0.5 dpa; 400°C, 0.3 dpa and 500°C, 0.5 dpa irradiations. The second column gives the expected effect on grain boundary Cr concentration if stage position 1 had a lower temperature than stage position 5. The third column provides the measured difference. For the 500°C, 0.5 dpa samples, stage position 1 shows greater grain boundary Cr concentration than stage position 5, contrary to the model predictions. Therefore, sample-to-sample differences cannot be explained by a systematic temperature difference across the stage.

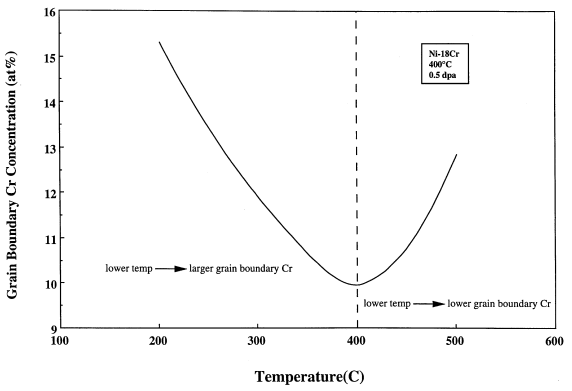

Fig. 9. The effect of temperature on model predicted grain boundary Cr concentration for a Ni–18Cr alloy. The minimum concentration occurs near 400°C.

Differences in irradiation temperature between samples are not expected to be responsible for the differences in segregation because temperature data from thermocouple readings and pyrometer readings taken during the irradiation indicated temperature differences of only ±10°C. An estimate of the variability in temperature needed to explain the differences in Cr depletion from sample-to-sample can be obtained from Fig. 9. The difference in average grain boundary concentration from 300°C to 400°C is 1.6 at.% and from 400°C to 500°C is

Table 4
Effect of irradiation temperature on segregation in Ni–18Cr

Irradiation condition (temp., dpa)	Expected effect on Cr concentration if stage position 1 is at lower temperature than stage position 5	Measured difference in Cr concentration
200°C, 0.5	$Cr_{pos1} > Cr_{pos5}$	$Cr_{pos1} > Cr_{pos5}$
300°C, 0.5	$Cr_{pos1} > Cr_{pos5}$	$Cr_{pos1} > Cr_{pos5}$
400°C, 0.3	$Cr_{pos1} > Cr_{pos5}$	$Cr_{pos1} > Cr_{pos5}$
500°C, 0.5	$Cr_{pos1} < Cr_{pos5}$	$Cr_{pos1} > Cr_{pos5}$

2.8 at.%. The measured difference in grain boundary Cr concentration between sample pairs ranges from 0.7 to 3.1 at.%. Thus, explaining the differences in sample average using variations in temperature from sample-to-sample would require temperature variations of nearly 25–100°C. Temperature differences of this magnitude were not seen during irradiation. Finally, the samples irradiated at 400°C to 0.5 dpa with average grain boundary Cr concentrations of 8.98 and 9.82 at.% are AES samples that were sectioned from an irradiated TEM bar (and therefore had equal temperature and dose histories). These samples have differences in average grain boundary Cr concentration comparable to many samples irradiated in different portions of the stage. Therefore, sample-to-sample differences do not appear to correlate with temperature.

5.3. Sample preparation history

Differences in sample-to-sample averages do not correlate with experimental temperature or dose, so the variability could be inherent to the material analyzed. If samples irradiated to the same dose at the same temperature have different segregation behavior, the types of grain boundaries in each sample could be different. The sample preparation process could produce samples whose grain boundaries exhibit different segregation behavior even at the same temperature and dose. If each sample has an inherently different segregation behavior, then the spread of the segregation data about the average would also be expected to be different. In this section, the variation of Ni–18Cr and Fe–20Cr–9Ni is studied to examine the spread of the data about the average.

As outlined above, the difference in sample-to-sample variation can be studied using an *F*-test. The *F*-test examines the variation or spread in the measurements. Table 5 shows the results of *F*-tests for the Ni–18Cr and Fe–20Cr–9Ni alloys. For each sample pair in Table 5, the sample variances, the test statistic Φ, and the confidence interval are listed. If the test statistic Φ lies within the confidence interval F_α, then the sample variations are statistically equal. Both alloys show consistency in the variance from sample-to-sample. For most cases, the variation of the concentration measurements from sample-to-sample irradiated at the same experimental conditions are not statistically different. The comparison of variance indicates that the majority of Ni–18Cr and Fe–20Cr–9Ni samples are from the same population. Since the variation is the same from sample-to-sample, the sample preparation process does not appear to produce samples with inherently different segregation behavior. Special care is taken to ensure preparation of the samples does not lead to variability. For a given alloy, all samples are taken from the same lot of material. Additionally, for samples on a given irradiation stage, all samples are bundled together during heat treatment so that each has the same temperature history.

Since systematic differences in temperature, dose, and alloy cannot uniquely explain the differences in sample-to-sample averages for the Ni–18Cr and Fe–20Cr–9Ni alloys, the differences must come from the mechanism of segregation or a non-systematic combination of temperature, dose, and boundary type.

6. Mechanistic implications associated with variability

Intrinsic material characteristics can cause variability in measured segregation. Grain boundary composition measurements (AES) from the Fe–20Cr–9Ni alloy will be used to examine this type of variability. By comparing only AES measurements, any variability due to measurement technique is normalized. Only irradiation conditions for Fe–20Cr–9Ni that have passed both the *t*- and *F*-tests will be examined. This ensures that no statistical differences in mean or variance exist between groups of measurements being studied.

6.1. Compositional inhomogeneity

Compositional inhomogeneity is proposed as a possible significant cause of variability in grain boundary compositions. Measurements falling far outside the standard deviation are typical of scatter caused by compositional inhomogeneity [11]. Fig. 10 plots the kurtosis for the chromium, nickel, and iron concentrations in Fe–20Cr–9Ni. The kurtosis is calculated from the bulk composition distributions, the unirradiated grain boundary distributions, and the distributions of boundaries irradiated to 3 dpa. In each case, the kurtosis is calculated from concentrations calculated from AES measurements. The kurtosis is plotted relative to that of a normal distribution. Therefore, positive values indicate a sharper peak than a normal distribution and negative values indicate a flatter distribution than a normal distribution. The bulk composition distributions all have positive kurtosis while the kurtosis from the unirradiated grain boundary compositions are all negative. At 3 dpa, both the chromium and iron distribution still have negative kurtosis. Since the kurtosis of the chromium and iron distributions in the unirradiated bulk material is positive (sharply peaked) but the kurtosis of the chromium and iron distribution on grain boundaries is negative (flatter), the chromium and iron segregation is not primarily driven by the bulk composition. The nickel distribution does have a positive kurtosis at 3 dpa, indicating that the grain boundary composition distribution may be related to the bulk composition distribution.

Table 5
Statistical analysis of sample variance in the Ni–18Cr and Fe–20Cr–9Ni alloys

Irradiation condition	Sample 1 variance	Sample 2 variance	Test statistic Φ	Confidence interval F_α (95%)	Are sample variances statistically equal ($\Phi < F_\alpha$)
Ni–18Cr (*temp.*, *dpa*)					
400°C, 0.1	5.42	0.52	10.37	2.74	No
400°C, 0.3	2.43	0.50	4.82	2.81	No
400°C, 0.5	2.46	1.60	1.54	4.48	Yes
400°C, 0.5	2.46	1.95	1.26	3.58	Yes
400°C, 0.5	2.46	1.36	1.81	3.41	Yes
400°C, 0.5	2.46	1.35	1.81	3.41	Yes
400°C, 0.5	1.95	1.60	1.22	3.77	Yes
400°C, 0.5	1.60	1.36	1.17	3.06	Yes
400°C, 0.5	1.60	1.35	1.18	3.06	Yes
400°C, 0.5	1.95	1.36	1.43	2.84	Yes
400°C, 0.5	1.95	1.35	1.44	2.84	Yes
400°C, 0.5	1.36	1.35	1.00	2.86	Yes
400°C, 1.0	2.55	2.44	1.05	2.84	Yes
200°C, 0.5	1.92	0.69	2.79	3.33	Yes
300°C, 0.5	1.31	1.16	1.12	2.99	Yes
500°C, 0.5	4.97	4.40	1.13	3.87	Yes
Fe–20Cr–9Ni					
400°C, 0.1	2.44	0.96	2.54	3.75	Yes
400°C, 1.0	1.09	1.79	1.64	2.86	Yes
400°C, 1.0	1.09	2.99	2.73	2.88	Yes
400°C, 1.0	1.09	1.57	1.44	2.86	Yes
400°C, 1.0	1.09	4.96	4.54	2.86	No
400°C, 1.0	1.79	2.99	1.67	3.20	Yes
400°C, 1.0	1.79	1.57	1.14	3.28	Yes
400°C, 1.0	1.79	4.96	2.77	3.28	Yes
400°C, 1.0	2.99	1.57	1.90	3.20	Yes
400°C, 1.0	2.99	4.96	1.66	3.05	Yes
400°C, 1.0	1.57	4.96	3.15	3.28	Yes
400°C, 3.0	2.29	3.46	1.52	2.63	Yes

6.2. Chromium distributions and grain boundary cracking

Estimates from percolation theory [18] suggest that 20–25% of grain boundaries need to be depleted below the threshold chromium concentration for intergranular stress corrosion cracking to occur. Fig. 10 shows that the grain boundary chromium distributions in the Fe–20Cr–9Ni alloy tend to be flatter than a normal distribution (negative kurtosis). If IASCC occurs when the grain boundary Cr falls below a threshold concentration and if the average grain boundary chromium concentration is greater than this threshold value, then a flat distribution has a greater number of boundaries with chromium concentrations less than the threshold value than does a peaked distribution (see Fig. 11). For this case, a flat distribution is more susceptible to environmental cracking than a peaked distribution with the same average chromium concentration. For an

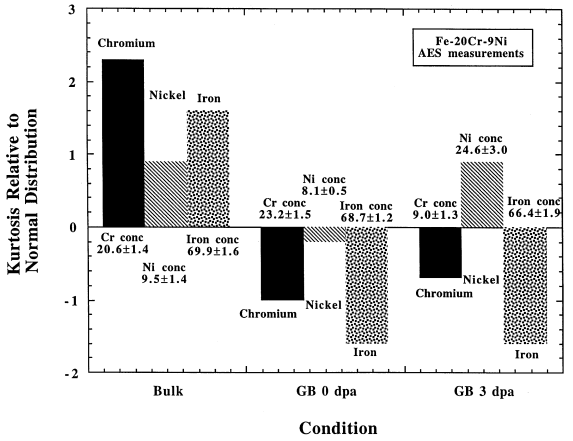

Fig. 10. Kurtosis (measure of peakedness) as a function of location and dose for Fe–20Cr–9Ni.

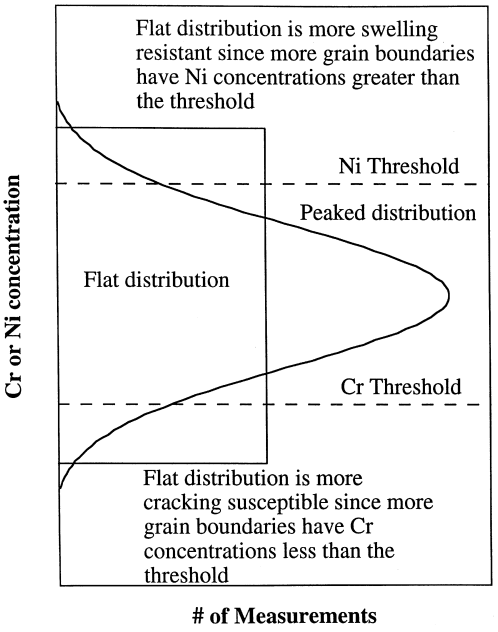

Fig. 11. For the same average concentrations, the shape of the distribution determines the number of boundaries below a threshold value.

average chromium concentration less than the critical value, a peaked distribution is more susceptible to environmental cracking. Therefore, in looking for solutions to irradiation assisted environmental cracking in water cooled reactors, methods which produce a more peaked distribution in chromium concentration while maintaining the average chromium concentration greater than a critical value will improve cracking resistance.

6.3. Nickel distributions and swelling

Fig. 10 shows that nickel distributions in the irradiated Fe–20Cr–9Ni alloy are more sharply peaked (positive kurtosis) than a normal distribution. Those alloys with greater nickel enrichment have been shown to be less prone to void swelling [19]. If a critical nickel concentration exists above which swelling becomes less likely and if the average nickel concentration is less than this critical value, then a flat distribution has a greater number of boundaries with nickel concentrations greater than the critical value than does a peaked distribution. For this case, a flat distribution is less susceptible to swelling than a peaked distribution with the same average nickel concentration (see Fig. 11). For an average nickel concentration greater than the critical value, a peaked distribution is less susceptible to swelling. Therefore, in looking for solutions to swelling in advanced reactors, methods which produce a more peaked distribution in nickel concentration while maintaining the average nickel greater than a critical value will improve swelling resistance.

6.4. The shape of the chromium and nickel distributions

As seen in Fig. 10, for irradiated grain boundaries the kurtosis of the nickel distribution is positive and the kurtosis of the chromium and iron distributions are negative. The nickel distribution is more sharply peaked, with the grain boundary nickel concentration clustering around a narrower band of values than the chromium and iron distributions. Carter et al. [12] have shown that Ni profiles in an ultra-high purity Fe–20Cr–9Ni alloy are 2–3 nm narrower than Cr and Fe profiles. The intensity of the Auger electrons follows the form

$$I(x) = I(0)\,\mathrm{e}^{-\lambda x},$$

where λ is the escape depth. If the Ni enrichment is modeled approximately as

$$C_{\mathrm{Ni}}(x) = C_{\mathrm{bulk}} + (C_{\mathrm{gb}} - C_{\mathrm{bulk}})\,\mathrm{e}^{-kx},$$

where k determines the profile width, then the intensity of Auger electrons measured at the grain boundary is given by

$$I_{\mathrm{gb}}^{\mathrm{meas}} = \frac{\int_0^\infty C_{\mathrm{Ni}}(x) I(x)\,\mathrm{d}x}{\int_0^\infty I(x)\,\mathrm{d}x} = C_{\mathrm{bulk}} + (C_{\mathrm{gb}} - C_{\mathrm{bulk}})\frac{\lambda}{\lambda + k}.$$

We can calculate the sensitivity of the measured grain boundary intensity with respect to the profile width (as determined by the constant k)

$$\frac{\mathrm{d}I_{\mathrm{gb}}^{\mathrm{meas}}}{\mathrm{d}k} = (C_{\mathrm{gb}} - C_{\mathrm{bulk}})\frac{-\lambda}{(\lambda + k)^2}.$$

The narrower the profile (the larger k), the less sensitive the measured Auger electron intensity is to changes in the profile width. Therefore, since Ni profiles tend to be narrower than Cr or Fe profiles, the concentrations calculated from AES measurements would be expected to have less variability. This is seen in the more sharply peaked profiles (positive kurtosis) for nickel.

7. Conclusions

The variability in grain boundary chromium concentration in irradiated samples was examined. The larger variability in AES measurements as compared to

STEM-EDS measurements is caused by the method by which the concentrations are calculated. Because concentrations calculated from AES measurements are sensitive to changes in the shape of the energy intensity peak and concentrations calculated from STEM-EDS measurements are not, the AES measurements have a greater variability. Because the scatter in AES data tends to be larger than in STEM-EDS, studies using AES should strive to obtain greater numbers of measurements to define a good statistical average.

Variability between samples irradiated to the same dose and at the same temperature was also examined, and a methodology for using statistical comparisons was outlined. This methodology provides a statistical comparison of calculated concentrations that allows investigation of systematic differences in experimental conditions such as temperature and dose. For the measurements in this work, the methodology shows that the variability in calculated concentrations between samples does not correlate with any systematic bias in the irradiation temperature, dose, or material condition. This statistical technique can be used with any data set to increase confidence in comparing data from separate samples with ostensibly the same history.

The distribution of concentration measurements was examined to gain an understanding of the segregation process. An examination of the kurtosis (peakedness) of the concentration distributions for iron, chromium, and nickel in irradiated Fe–20Cr–9Ni showed that this alloy could be made less susceptible to environmental cracking and void swelling by controlling both the average chromium and nickel concentration and the shape of the concentration distributions.

Acknowledgements

The authors gratefully acknowledge J.M. Cookson, D. Damcott, R.D. Carter, J. Gan, and J.T. Busby for assistance in performing sample irradiations and to the Michigan Ion Beam Laboratory at the University of Michigan for the use of the irradiation facilities. We also thank the Surface Analysis Laboratory at the Ford Motor Company Research and Development Center for the use of their PHI 660 Scanning Auger Microprobes. Additional thanks go to the Electron Microbeam Analysis Laboratory and staff at the University of Michigan. Finally, thanks go out to S.M. Bruemmer at Pacific Northwest Laboratory for his support. Work supported under contract W-31-109-Eng-38 with the Department of Energy. This research was also supported by the US Department of Energy under grant DE-FG02-93ER-12310, by the Associated Western Universities-Northwest under US Department of Energy grant DE-FG02-89ER-7552, and by the Southeast Universities Research Association, Inc. through the SURA/ORNL summer research program. Research partially supported by the Division of Materials Sciences, US Department of Energy under contract DE-AC05-96OR22464 with Lockheed Martin Energy Research Corp., and through the SHaRE Program under contract DE-AC05-76OR00033 with Oak Ridge Associated Universities.

References

[1] A.J. Jacobs, in: A.S. Kumar, D.S. Gelles, R.K. Nanstad, E.A. Little (Eds.), Proceedings of the 16th Internationl Symposium on Radaition on Materials, ASTM-STP 1175, American Society for Testing and Materials, Philadelphia, 1993, p. 902.
[2] T. Kato, H. Takahashi, M. Izumiya, J. Nucl. Mater. 189 (1992) 167.
[3] D.I.R. Norris, C. Baker, C. Taylor, J.M. Titchmarsh, in: R.E. Stoller, A.S. Kumar, D.S. Gelles (Eds.), Fifteenth International Symposium, ASTM STP 1125, American Society for Testing and Materials, 1992, p. 603.
[4] K. Nakata, I. Masaoka, J. Nucl. Mater. 150 (1987) 186.
[5] S. Dumbill, PhD thesis, University of Birmingham, 1992.
[6] S. Dumbill, T.M. Williams, in: Proceedings of the Conference on Materials for Nuclear Reactor Core Applications, vol. 1, BNES, London, 1987, p. 119.
[7] S. Watanabe, H. Kinoshita, N. Sakaguchi, H. Takahashi, J. Nucl. Mater. 226 (1995) 330.
[8] D.L. Damcott, T.R. Allen, G.S. Was, J. Nucl. Mater. 225 (1995) 97.
[9] T.R. Allen, G.S. Was, E.A. Kenik, J. Nucl. Mater. 255 (1998) 44.
[10] G.S. Was, T.R. Allen, J.T. Busby, J. Gan, D. Damcott, D. Carter, M. Atzmon, E.A. Kenik, J. Nucl. Mater. 270 (1999) 96.
[11] C.L. Briant, Acta Met. 31 (1983) 257.
[12] R.D. Carter, D.L. Damcott, M. Atzmon, G.S. Was, S.M. Bruemmer, E.A. Kenik, J. Nucl. Mater. 211 (1994) 70.
[13] T.R. Allen, G.S. Was, E.A. Kenik, in: Proceedings of the Seventh International Symposium on Env. Deg. of Materials in Nuclear Power Systems-Water Reactors, Breckenridge, CO, 1995, NACE International, Houston, TX, p. 997.
[14] L.E. Davis, N.C. MacDonald, P.W. Palmberg, G.E. Riach, R.E. Weber, Handbook of Auger Electron Spectroscopy, second ed., Perkin–Elmer, Eden Prairie, MN.
[15] W. Mendenhall, Introduction to Probability and Statistics, PWS, Boston, MA, 1987.
[16] I.F. Ferguson, Auger Microprobe Analysis, Adam Hilger, Bristol, 1989.
[17] P.H. Holloway, Scanning Electron Microsc. 1 (1978) 361.
[18] D.B. Wells, J. Stewart, A.W. Herbert, P.M. Scott, D.E. Williams, The use of percolation theory to predict

the probability of failure of sensitised, Austenitic Stainless Steels by Intergranular Stress Corrosion Cracking, Harwell Laboratory, Oxfordshire, England, AERE-R12903, 1987.

[19] T.R. Allen, J.T. Busby, J. Gan, E.A. Kenik, G.S. Was, The correlation between swelling and radiation-induced segregation in Fe–Cr–Ni alloys, submitted to 19th Symposium on Effects of Radiation on Materials.